Structural and magnetic phases of $Fe(ND_3)_2PO_4$

2008 J. Phys.: Condens. Matter 20 104227

(http://iopscience.iop.org/0953-8984/20/10/104227)

J. Phys.: Condens. Matter **20** (2008) 104227 (6pp) doi:10.1088/0953-8984/20/10/104227

Structural and magnetic phases of $Fe(ND_3)_2PO_4$

B F Alfonso[1], C Trobajo[2], M A Salvadó[3], P Pertierra[3], S García-Granda[3], J Rodríguez-Fernández[4], M T Fernández-Díaz[5], J A Blanco[1,6] and J R García[2]

[1] Departamento de Física, Facultad de Ciencias, Universidad de Oviedo, 33007 Oviedo, Spain
[2] Departamento de Química Orgánica e Inorgánica, Facultad de Químicas, Universidad de Oviedo, 33006 Oviedo, Spain
[3] Departamento de Química Física y Analítica, Facultad de Químicas, Universidad de Oviedo, 33006 Oviedo, Spain
[4] CITIMAC, Facultad de Ciencias, Universidad de Cantabria, 39005 Santander, Spain
[5] Institute Laue-Langevin, BP 156X, F-38042, Grenoble, France

E-mail: jabr@uniovi.es

Received 14 July 2007
Published 19 February 2008
Online at stacks.iop.org/JPhysCM/20/104227

Abstract

Polycrystalline samples of $Fe(ND_3)_2PO_4$ were prepared by means of a hydrothermal route and characterized using powder x-ray diffraction, scanning electron microscopy, chemical and thermal analysis, magnetic measurements, specific heat and neutron diffraction experiments. This material orders within an orthorhombic (*Pnma* space group) crystal structure at room temperature, but below 220 K the crystal structure changes towards a monoclinic $P2_1/n$ structure through a phase transition with almost no latent heat. Furthermore, the magnetic cell at 2 K is twice the size of the crystallographic cell observed at 80 K. The magnetic structure associated with the Fe(III) ions is thus commensurate with the crystal lattice having a propagation vector $\vec{k} = (1/2, 0, 0)$, the magnetic moments lying in the yz plane of the crystallographic cell.

(Some figures in this article are in colour only in the electronic version)

1. Introduction

Inorganic materials with an open framework are of particular interest because of their applications in fields such as heterogeneous catalysis, ion exchange, sensors and nanotechnology. At the beginning of the 1980s the synthesis and structural characterization of novel open-framework solids was profusely reported and among these, the family of phosphates is quite large [1, 2]. The continuing interest in open-framework transition metal phosphates is basically due to the possibility of investigating the interplay of structure, dimensionality and magnetism. Iron phosphates occupy an important position in this interesting class of compounds, they exhibit at the same time physical properties such as conductivity and magnetic and optical features. Nowadays many potential applications in the field of catalysis, waste purification systems, ferroelectrics, lithium batteries etc continue to be the driving force for research in open-framework solids [3–6].

Iron(III) phosphates exist as minerals and have a rich crystal chemistry. These minerals are often basic and/or hydrated phosphates and belong to the most perplexing substances in the mineral kingdom [7]. Synthetic iron(III) phosphates are of particular interest by virtue of their structural chemistry and magnetic properties [8]. In a previous paper [9], we presented the direct synthesis of iron(III) phosphates under mild hydrothermal conditions by the reaction of $FeCl_3$(aq) and H_3PO_4(aq) in the presence of urea. The compound produced is very sensitive to the presence of urea in the reaction system and to its concentration. Without urea and at low urea concentrations, only $FePO_4 \cdot 2H_2O$ is formed. With an increase in the urea concentration, $NH_4Fe(HPO_4)$ is formed. Further increases in urea concentration, resulting in progressive neutralization of H_3PO_4 and an increase in

[6] Author to whom any correspondence should be addressed. Present address: Departamento de Física, Universidad de Oviedo, Campus de Llamaquique, 33005 Oviedo, Spain.

pH in the reaction media, provide favourable conditions for the formation of $NH_4Fe_2(PO_4)_2(OH)\cdot 2H_2O$. When the amount of urea added is very high, the ammonia molecules present in the reaction media act as template agents and a new compound, $Fe(NH_3)_2PO_4$, is formed. This compound is the only reported iron(III) phosphate containing ammonia molecules and, furthermore, is also the only three-dimensional structurally characterized solid containing Fe–NH_3 bonds [10].

The $Fe(NH_3)_2PO_4$ compound (orthorhombic, $Pnma$, at room temperature) is related to $FePO_4\cdot 2H_2O$, which is present in the mineral kingdom in two forms: strengite (orthorhombic, $Pbca$) and metastrengite, also called phosphosiderite (monoclinic, $P2_1/n$). This paper, which reports the structure of the monoclinic-$Fe(NH_3)_2PO_4$ form (stable at low temperature), is organized as follows: an experimental section (section 2) describes the synthesis of the material and the experimental methods used throughout this work. Section 3 presents the results and discussion of the neutron diffraction and magnetic susceptibility measurements. Finally, section 4, contains a number of remarks and our conclusions.

2. Experimental section

2.1. Synthesis and initial characterization

The synthesis of a deuterated sample was carried out by a hydrothermal route. The reagents used were $FeCl_3$ (Riedel-of Naën), D_3PO_4 (Aldrich, 85 wt% solution in D_2O), $(ND_2)_2CO$ (Aldrich, 98% atom D) and D_2O (Merck 99.8%). 4 g of $FeCl_3$ were dissolved in 25 ml of D_2O and mixed with D_3PO_4 and $(ND_2)_2CO$ in a molar ratio C/P = 2 and P/Fe = 10. The total volume of the reaction mixture was 40 ml. The mixing was carried out in a stainless steel (100 ml) Teflon-lined vessel under autogenous pressure. The autoclave was sealed and heated to 180 °C for six days. The solid product was filtered off, thoroughly washed with an excess of D_2O and dried in air at room temperature.

The iron phosphate, $Fe(NH_3)_2PO_4$, was also synthesized under hydrothermal conditions as reported in the literature [10].

2.2. Analytical procedures

The initial characterization was carried out using powder x-ray diffraction (XRD), thermogravimetric analysis (TGA), infrared measurements (IR) and scanning electronic microscopy (SEM). The powder XRD patterns were recorded using a Philips model PW 1050 conventional powder diffractometer (Cu Kα 40 kV and 30 mA). The data were collected at room temperature over the angular range 13°–110° 2θ with a step of 0.02° (time constant 10 s). Thermogravimetric analysis (TGA) was carried out on a Mettler TA 4000, model TG 50, at a rate of 10 °C min^{-1} in nitrogen atmosphere. The studies show weight losses in two overlapping steps, which begin gradually at about 250 °C and are complete at about 400 °C. The total weight loss corresponds to the two ammonia molecules. The infrared spectra were recorded on a Perkin-Elmer 1000 FT-IR spectrophotometer. Infrared spectroscopic studies carried out in the range 400–4000 cm^{-1} using the KBr pellet method exhibited typical peaks corresponding to the ammonia molecules, 3341 and 3253 cm^{-1} (free NH_3) and 1591 cm^{-1} (NH_3 asymmetric). The scanning electronic microscopy (SEM) image was obtained on a JEOL 6100, operating at 20 kV. The SEM image indicates that the compound has a fibrous morphology [9]. The (dc) magnetic susceptibility measurements were performed on polycrystalline samples under an applied magnetic field of 1 kOe in the temperature range $1.8 \leqslant T$ (K) $\leqslant 300$ using PPMS equipment belonging to the Servicio de Medidas Magnéticas of the University of Oviedo.

2.3. Powder neutron diffraction

Powder neutron diffraction patterns with constant-wavelength: $\lambda = 1.594$ Å were collected using the diffractometer D2B, operating in high-resolution mode at the Institute Laue-Langevin, Grenoble (France). The samples (deuterated and hydrogenated) were loaded into a cylindrical vanadium can, and the data were collected at 300, 80 and 2 K, in the two last cases using an orange cryostat and in all cases over the angular range of 10°–159° 2θ with a step size of 0.05°. The raw data were collected and normalized using local software routines.

3. Results and discussion

3.1. Analysis of the neutron diffraction data obtained at 300 K

Rietveld refinement was carried out using the program FULLPROF [11]. The starting atomic model, without H-atom positions, was the previous result from our x-ray powder study on $Fe(NH_3)_2PO_4$ [10]. First we refined the non-structural parameters (fifth-order polynomial background, scale factor, zero shift error and peak shape parameters for the pseudo-Voigt function), the cell parameters and a global isotropic temperature factor. At this point, a difference-Fourier synthesis was performed using SXELXL97 [12] and 'observed' F^2 from neutron refinement, showing the positions of all D atoms at the deepest holes. In subsequent cycles all the coordinates, including those of deuterium atoms, and isotropic displacement parameters were refined for each discrete atom type. Final refinement yielded good agreement factors and small profile differences. Figure 1(a) shows the neutron diffraction pattern and the difference between the calculated pattern, including the refined background, and the observed pattern. Crystallographic parameters are shown in table 1. Final coordinates, including deuterium atom positions and isotropic displacement parameters, are shown in table 2. All results are for the deuterium sample, as the hydrogen compound exhibits no significant differences.

3.2. Analysis of the neutron diffraction data obtained at 80 K

The sample undergoes a phase transition when the temperature is lowered from 300 K down to 2 K. Attempts to perform the indexation with the cell parameters associated with the room temperature phase were unsuccessful, but it was possible to index the new peaks using a monoclinic setting. A detailed examination of the powder neutron pattern allowed us to find a

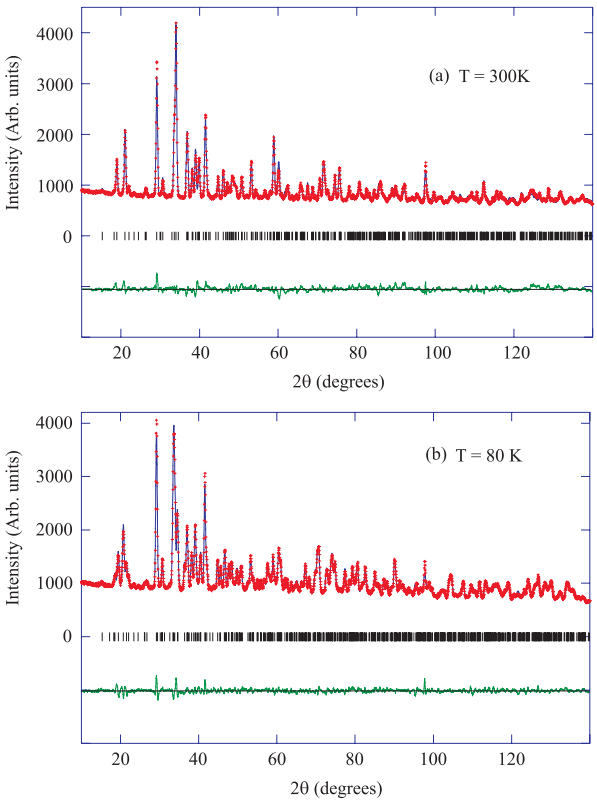

Figure 1. Powder neutron-diffraction pattern of $Fe(ND_3)_2PO_4$. Observed (+) and calculated (solid line) patterns collected (a) at 300 K and (b) at 80 K. Positions of the Bragg reflections are represented by vertical bars. The observed–calculated difference is depicted at the bottom of the figure.

Table 1. Crystal data and structure refinements for $FePO_4N_2D_6$ at 300 and 80 K.

	$Fe(ND_3)_2PO_4$ (300 K)		$Fe(ND_3)_2PO_4$ (80 K)
Empirical formula	$FePO_4N_2D_6$		$FePO_4N_2D_6$
Crystal system	Orthorhombic		Monoclinic
Space group	*Pnma*(#62)		$P2_1/n$(#14)
Z	4		4
	X-ray[a]	Neutron	Neutron
λ (Å)	1.5418	1.594	1.594
a (Å)	10.1058(2)	10.1094(4)	6.3607(3)
b (Å)	6.3676(2)	6.3691(3)	10.0927(4)
c (Å)	7.5714(2)	7.5709(5)	7.5690(3)
β (deg)	—	—	92.562(3)
V (Å^3)	487.21(2)	487.47(4)	485.41(4)
2θ range (deg)	13–110	10–140	10–140
Step	0.02	0.05	0.05
Parameters	38	46	62
No. soft constraints	—	2	—
R_{wp} [b]	12.3	3.47	3.17
R_{exp} [b]	6.1	1.51	1.38
R_F	5.6	7.3	2.5

[a] Data from *Inorg. Chem.,* [10].
[b] Background included.

splitting of some Bragg reflections (h, k, l) according to a lost symmetry. Subsequently, the structural relationship between the room temperature cell (orthorhombic, space group *Pnma* (# 62)) and the possible monoclinic cell were obtained [13]. The compatible monoclinic groups were $P2_1/c$, $P2_1/m$ or $P2_1/n$. The agreement of the calculated versus observed patterns was slightly better for the space group $P2_1/n$ (# 14). At this stage, the same strategy as in the previous compound was used to locate hydrogen atom positions. Final refinement yielded good agreement factors and small profile difference, as can be seen in figure 1(b). Final coordinates including deuterium atom positions and isotropic displacement parameters are given in table 3, while bond distances and selected angles are shown in table 4.

Table 2. Fractional atomic coordinates and isotropic displacement parameters (Å^2) for $Fe(ND_3)_2PO_4$ at 300 K.

Atom	Wyckoff position	x	y	z	B
Fe	4c	0.8443(4)	0.750 00	0.0926(5)	0.82(6)
P	4c	0.1635(9)	0.750 00	0.0428(9)	1.5(1)
O1	8d	0.1643(5)	0.5612(6)	−0.0808(6)	1.49(7)
O2	4c	0.2824(7)	0.750 00	0.163(1)	1.49(7)
O3	4c	0.0328(6)	0.750 00	0.1514(9)	1.49(7)
N1	4c	0.6483(5)	0.750 00	−0.0124(6)	2.02(7)
D11	8d	0.6258(7)	0.6225(9)	−0.0890(8)	5.3(1)
D12	4c	0.5684(9)	0.750 00	0.085(1)	5.3(1)
N2	4c	0.8975(5)	0.750 00	−0.1852(8)	2.0(7)
D21	8d	0.0465(6)	0.377(1)	0.2109(9)	5.3(1)
D22	4c	0.821(1)	0.750 00	−0.272(2)	5.3(1)

Table 3. Fractional atomic coordinates and isotropic displacement parameters (Å^2) for $Fe(ND_3)_2PO_4$ at 80 K.

Atom	Wyckoff position	x	y	z	B
Fe	4e	0.2556(7)	0.3422(4)	0.5886(5)	0.24(7)
P	4e	0.259(1)	0.6670(9)	0.546(1)	2.08(2)
O1a	4e	0.5612(9)	0.8482(6)	0.9166(8)	0.42(5)
O1b	4e	0.433(1)	0.6790(6)	0.4200(8)	0.42(5)
O2	4e	0.227(1)	0.7801(6)	0.6588(9)	0.42(5)
O3	4e	0.265(1)	0.5331(6)	0.6588(9)	0.42(5)
N1	4e	0.2293(7)	0.1410(5)	0.4868(6)	1.14(6)
D11a	4e	0.842(1)	0.3750(8)	0.8997(9)	2.24(6)
D11b	4e	0.098(1)	0.1311(7)	0.4168(9)	2.24(6)
D12	4e	0.236(1)	0.0718(7)	0.593(1)	2.24(6)
N2	4e	0.2350(8)	0.3939(5)	0.3177(7)	1.14(6)
D21a	4e	0.362(1)	0.9761(7)	0.201(1)	2.24(6)
D21b	4e	0.617(1)	0.5662(8)	0.7206(9)	2.24(6)
D22	4e	0.315(1)	0.8206(7)	0.271(1)	2.24(6)

3.3. Crystal structure analysis

The structure of $Fe(ND_3)_2PO_4$ at 300 K can be described by a metal-centred octahedron $[FeO_4N_2]$ linked together via $[PO_4]$ a tetradentate tetrahedron to form a three-dimensional network. Two crystallographically independent ammonia molecules in relative cis position complete the octahedral environment of the iron atom. The channels along the b axis are fully occupied by the ammonia molecules. There is only one crystallographically independent iron per unit cell. A projection of the crystal structure at room temperature along the b axis is shown in figure 2. Below 220 K, the orthorhombic crystal structure changes towards a monoclinic $P2_1/n$ structure through a phase

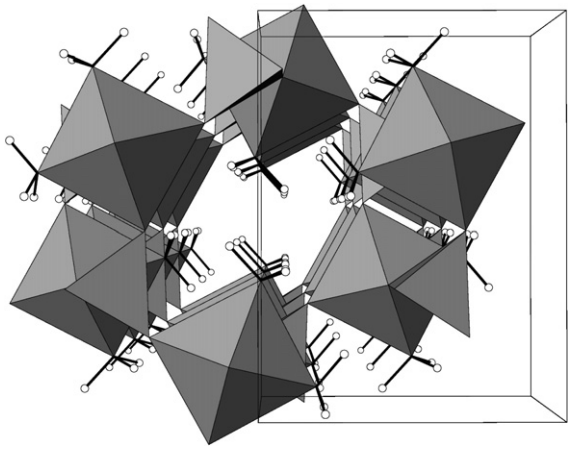

Figure 2. View of the crystal structure of $Fe(ND_3)_2PO_4$ along the *b* axis.

Table 4. Selected bond distances (Å) and angles (deg) for $Fe(ND_3)_2PO_4$ at 80 K.

Fe–O1a	2.015(7)	O1a–Fe–O1b	174.6(6)
Fe–O1b	1.993(8)	O1a–Fe–O2	92.3(5)
Fe–O2	2.010(8)	O1a–Fe–O3	89.6(5)
Fe–O3	1.991(7)	O1a–Fe–N1	87.7(4)
Fe–N1	2.177(6)	O1a–Fe–N2	87.7(4)
Fe–N2	2.114(6)	O1b–Fe–O2	89.1(5)
		O1b–Fe–O3	95.4(5)
P–O1a	1.57(1)	O1b–Fe–N1	87.1(4)
P–O1b	1.50(1)	O1b–Fe–N2	87.1(4)
P–O2	1.45(1)	O2–Fe–O3	90.8(4)
P–O3	1.58(1)	O2–Fe–N1	93.6(5)
		O2–Fe–N2	176.1(5)
N1–D11a	1.011(8)	O3–Fe–N1	173.3(5)
N1–D11b	0.975(9)	O3–Fe–N2	90.3(4)
N1–D12	1.065(9)	N1–Fe–N2	83.5(3)
N2–D21a	1.040(9)	O1a–P–O1b	102.1(8)
N2–D21b	1.078(9)	O1a–P–O2	108.4(8)
N2–D22	1.039(9)	O1a–P–O3	104.0(8)
		O1b–P–O2	116.1(8)
		O1b–P–O3	113.6(8)
		O2–P–O3	11.4(8)
		D11a–N1–D11b	104(1)
		D11a–N1–D12	113(1)
		D11b–N1–D12	110(1)

transition with almost no latent heat [15]. Basic structural features are maintained although symmetry is lost at the expense of strong hydrogen bonds.

Figure 3 shows a projection of the orthorhombic (a) and the monoclinic (b) crystal structures.

3.4. Magnetic susceptibility measurements

The temperature variation of the molar magnetic susceptibility, χ_M, in the temperature range $1.8 \leqslant T(K) \leqslant 300$ is shown in figure 4(a), while the inset shows the same variation up to 50 K. χ_M increases with decreasing temperature, reaching a slightly broad maximum around 28 K above the Néel temperature, $T_N = 22$ K, which could be related to short-range order or two-dimensional magnetism, after which χ_M decreases below T_N. When the temperature is lowered further, χ_M

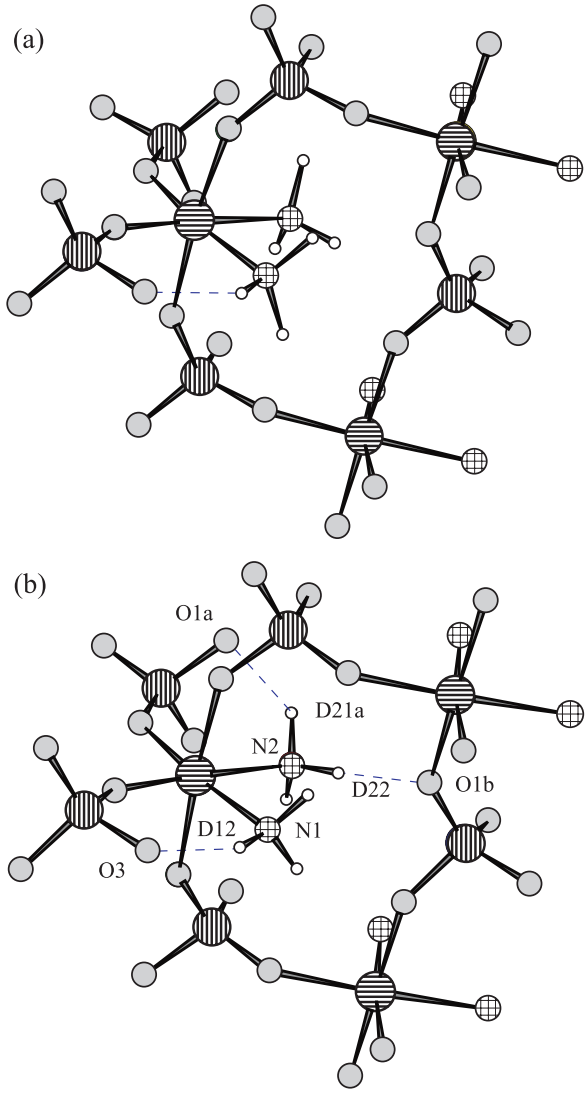

Figure 3. (a) Orthorhombic crystal structure, (b) monoclinic crystal structure of $Fe(ND_3)_2PO_4$. Fe: horizontal line, P: vertical line, N: horizontal–vertical line, O: solid circles and D: empty circles.

decreases sharply. At high temperatures ($T > 100$ K), on the other hand, the temperature dependence of χ_M follows a Curie–Weiss law (see figure 4(b)), $\chi_M = C/(T - \theta_P)$, with $C = 4.64(1)$ cm^3 K mol^{-1} and $\theta_P \approx -73$ K, where C is the Curie constant for the 3d-Fe^{3+} ion and θ_P is the paramagnetic Curie temperature. These values are in quite good agreement with data previously reported by Goñi *et al* [14]. They were obtained from a fit to the temperature dependence of its reciprocal molar magnetic susceptibilities, χ_M^{-1}. The observed effective magnetic moment (μ_{eff}) saturates to a value of 6.09(1) μ_B, which is close to the expected one associated with the paramagnetic spin-only value of Fe in a +3 state (5.92 μ_B). The negative paramagnetic Curie–Weiss temperature implies that the dominant interactions between the neighbouring Fe^{+3} species are antiferromagnetic.

3.5. Magnetic structure

Neutron diffraction profile of the $Fe(ND_3)_2PO_4$ compound measured at 2 K is shown in figure 5. From the comparison

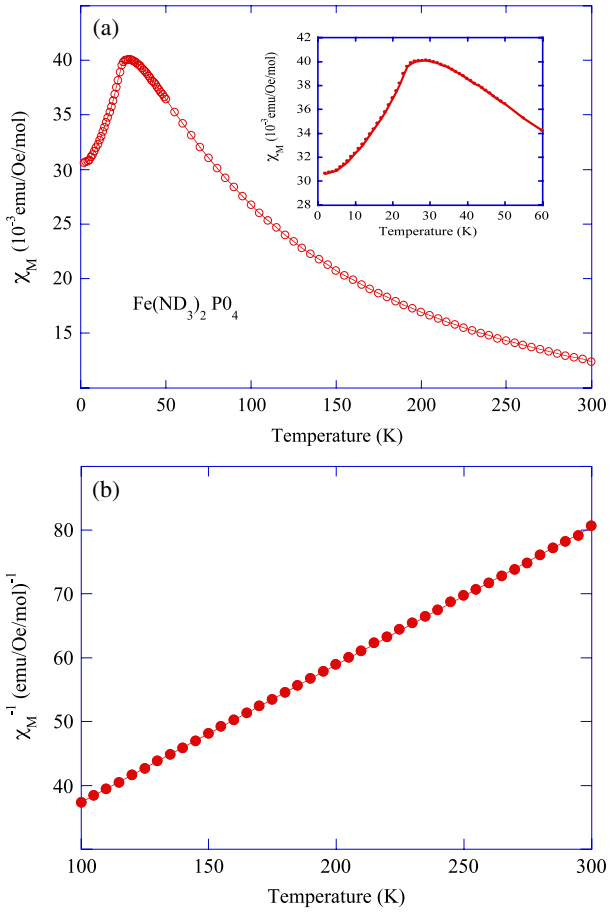

Figure 4. (a) Temperature dependence of the molar magnetic susceptibility χ_M of $Fe(ND_3)_2PO_4$. The inset shows a detail of χ_M in the range of temperatures from 1.8 K up to 60 K. (b) Temperature dependence of the reciprocal molar magnetic susceptibility χ_M^{-1}. The solid line corresponds to a fit to a Curie–Weiss law (see text).

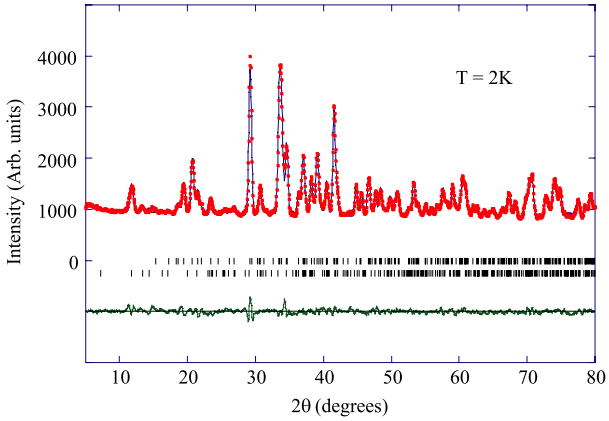

Figure 5. Powder neutron-diffraction pattern of $Fe(ND_3)_2PO_4$. Observed (+) and calculated (solid line) patterns collected at 2 K. Positions of the Bragg reflections are represented by vertical bars. The first row corresponds to the nuclear peaks, while the second is associated with the magnetic peaks. The observed–calculated difference is depicted at the bottom of the figure.

Table 5. Atomic coordinates (Å) and magnetic moments (μ_B) of the Fe(III) ions determined from powder neutron diffraction patterns collected at 2 K. The total magnetic moment is around 3.7 μ_B for the $Fe(ND_3)_2PO_4$ at 2 K.

Atom	x	y	z	M_x	M_y	M_z
Fe1	0.254 19(9)	0.343 18(6)	0.589 14(7)	0	−2.09(7)	3.05(8)
Fe2	0.245 81(9)	0.843 18(6)	0.910 86(7)	0	2.09(7)	−3.05(8)
Fe3	0.745 81(9)	0.656 82(6)	0.410 86(7)	0	−2.09(7)	3.05(8)
Fe4	0.754 19(9)	0.156 82(6)	0.089 14(7)	0	2.09(7)	−3.05(8)

with the diffraction pattern collected at 80 K (see figure 1(b)), the appearance of new additional magnetic peaks is clearly observed. The most important one, at around 11° in 2θ, indicates that the system is magnetically ordered, as was suggested above by the magnetic measurements. As the intensity of the magnetic reflections are rather weak and the number of these is not large, the determination of the magnetic structure in a powder sample is not a straightforward task (a similar situation can be found in [16, 17]) and no single solution is assured.

The magnetic structure could be described by means of a propagation vector $\vec{k} = (1/2, 0, 0)$, which means that the magnetic cell is twice the size of the nuclear cell along the crystallographic a-axis. As mentioned above, the Fe(III) magnetic ions of the cell are distributed over equivalent positions of the crystallographic site at the special Wyckoff position 4e with $x = 0.254\,19(9)$, $y = 0.343\,18(6)$ and $z = 0.589\,14(7)$. These values were obtained from the refinement of the nuclear peaks of the neutron pattern registered at 2 K. The arrangement of magnetic moments was found with the help of group-theory calculations. The different magnetic arrangements were then investigated, checking all the different basis functions of the irreducible representations of the $P2_1/n$ space group for the propagation vector $\vec{k} = (1/2, 0, 0)$ and using the Basireps package distributed on the Fullprof-suite platform [18]. This method, based on Bertaut's symmetry analysis [19], allows us to determine the symmetry constraint of the four Fe(III) ions located at the 4c Wyckoff site symmetry. The total Γ representation of the propagation vector group G_k can be decomposed upon the irreducible representations $\Gamma = 6\Gamma_1$ which leads to basis functions of representation Γ_1 of dimension 2 contained six times in Γ. These basis functions separate the Fe(III) magnetic sublattice into two sets of related magnetic moments: atoms 1 and 2, and atoms 3 and 4 (see table 5). For each combination of basis function, we have carried out a systematic comparison between the observed and calculated neutron diffraction patterns at 2 K. From this analysis, the direction of the magnetic moments seems to lie in the yz plane. The best agreement is found when the magnetic moments are arranged according to the sequence $-G_yG_z$ in Bertaut's notation; G means $(+\,-\,+-)$ for atoms 1, 2, 3 and 4, respectively. The magnetic moment was defined using spherical coordinates and these were refined by the modulus of the magnetic moment and the angle ϕ with the z direction, imposing the condition of equality of the magnetic moments associated with the two sets of atoms mentioned above. The best fit ($R_B \sim 18\%$) to the experimental pattern at 2 K is shown in figure 6. The modulus of the magnetic moment of the Fe(III) ions is 3.7 μ_B and the angle ϕ is around 34.5°.

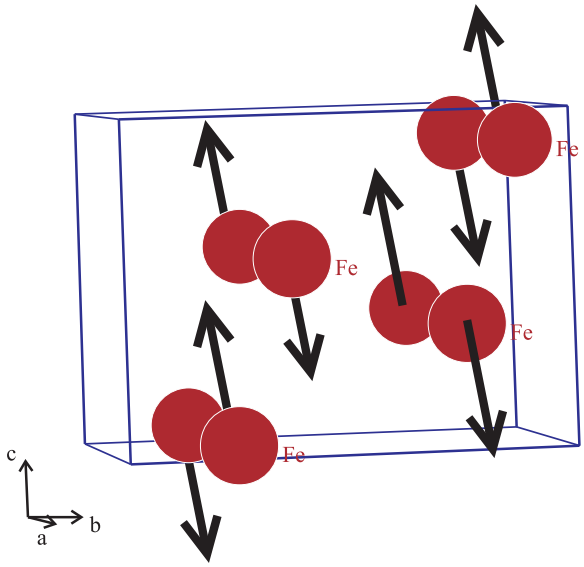

Figure 6. Representation of the magnetic structure of $Fe(ND_3)_2PO_4$ at 2 K.

A schematic representation of the magnetic arrangements is shown in figure 6. The magnetic moments from one unit to the next one along the a-axis are antiferromagnetically coupled.

4. Conclusions

The structural and magnetic phases of $Fe(ND_3)_2PO_4$ were determined from powder neutron diffraction experiments. The system undergoes two phase transitions: first a structural one from an orthorhombic crystal structure ($Pnma$ space group) at room temperature to a monoclinic structure ($P2_1/n$ space group) below 220 K; and second, below $T_N = 22$ K, it orders with an antiferromagnetic structure with a propagation vector $\vec{k} = (1/2, 0, 0)$, the magnetic moments lying in the yz-plane of the low temperature monoclinic crystal lattice. Recent heat capacity measurements show that the material undergoes two successive magnetic phase transitions just below T_N. This quite surprising behaviour underlines the competition of Fe–Fe interactions through the PO_4 groups involving Fe–O–P–O–P–Fe long range superexchange interactions. Further neutron diffraction experiments will elucidate this behaviour around T_N.

Acknowledgments

We are grateful for financial support from FEDER-MEC (MAT2005-06806-C04-01, MAT2006-13548-C02-02, MAT2006-01997 and Factoría Española de Cristalización-Consolider Ingenio-2010).

References

[1] Cheetham A K, Ferey G and Loiseau T 1999 *Angew. Chem. Int. Edn Engl.* **38** 3268–92
[2] Rajic N 2005 *J. Serb. Chem. Soc.* **70** 371–91
[3] Riou-Cavellec M, Riou D and Ferey G 1999 *Inorg. Chim. Acta* **291** 317–25
[4] Ai M 1999 *Catal. Today* **52** 65–9
[5] Song Y, Zavalij P Y, Suzuki M and Whittingham M S 2002 *Inorg. Chem.* **41** 5778–86
[6] Reale P, Scrosati B, Delacourt C, Wurm C, Morcrette M and Masquelier C 2003 *Chem. Mater.* **15** 5051–8
[7] Moore P B 1970 *Am. Miner.* **55** 135–69
[8] Choudhury A and Natarajan S 2000 *Int. J. Inorg. Mater.* **2** 217–23
[9] Trobajo C, Espina A, Jaimez E, Khainakov S A and García J R 2000 *J. Chem. Soc. Dalton Trans.* 787–90
[10] Salvadó M, A, Pertierra P, García-Granda S, Espina A, Trobajo C and García J R 1999 *Inorg. Chem.* **38** 5944–7
[11] Rodríguez-Carvajal J 1990 *FULLPROF: A Program for Rietveld Refinement and Pattern Matching Analysis (XV Congr. of the IUCr) (Toulouse, France)* p 127 (Abstracts of the Satellite Meeting on Powder Diffraction)
[12] Sheldrick G M 1997 *SHELXL97 Program for the Refinement of Crystal Structures* University of Göttingen, Germany
[13] Hahn T (ed) 2002 *International Tables for Crystallography* volume A *Space-Group Symmetry* 5th edn (Dordrecht: Kluwer)
[14] Goñi A, Lezama L, Espina A, Trobajo C, García J R and Rojo T 2001 *J. Mater. Chem.* **11** 2315–9
[15] Alfonso B F, Trobajo C, Salvadó M A, Pertierra P, García-Granda S, Rodríguez-Fernández J, Fernández-Díaz M T, Blanco J A and García J R 2007 at press
[16] Blanco J A, Espeso J I, García-Soldevilla J, Gómez-Sal J C, Ibarra M R, Marquina C and Fisher H E 1999 *Phys. Rev.* B **59** 512–8
[17] Espeso J I, García-Soldevilla, Blanco J A, Rodríguez Fernández J, Gómez-Sal J C and Fernández Díaz M T 2000 *Eur. Phys. J.* B **18** 625–32
[18] Rodriguez-Carvajal J 2007 BASIREPS: a program for calculating irreducible representations of space groups and basis functions for axial and polar vector properties (http://www.ill.fr/dif/Soft/fp/php/downloads.html)
[19] Bertaut E F 1968 *Acta Crystallogr.* A **24** 217–31